Importance of vegetation dynamics for future terrestrial carbon cycling

2015 Environ. Res. Lett. 10 054019

(http://iopscience.iop.org/1748-9326/10/5/054019)

Environmental Research Letters

LETTER

Importance of vegetation dynamics for future terrestrial carbon cycling

Anders Ahlström[1,2], **Jianyang Xia**[3,4], **Almut Arneth**[5], **Yiqi Luo**[3] **and Benjamin Smith**[1]

[1] Department of Physical Geography and Ecosystem Science, Lund University, Sölvegatan 12, SE-223 62 Lund, Sweden
[2] Department of Earth System Science, School of Earth, Energy and Environmental Sciences, Stanford University, Stanford, CA 94305, USA
[3] Department of Microbiology and Plant Biology, University of Oklahoma, 770 Van Vleet Oval, Norman, OK, USA
[4] Tiantong National Forest Ecosystem Observation and Research Station, School of Ecological and Environmental Sciences, East China Normal University, Shanghai 200062, People's Republic of China
[5] Institute for Meteorology and Climate Research—Atmospheric Environmental Research, Karlsruhe Institute of Technology, Kreuzeckbahnstrasse 19, D-82467 Garmisch-Partenkirchen, Germany

E-mail: anders.ahlstrom@nateko.lu.se

Keywords: vegetation dynamics, DGVM, LPJ-GUESS, CMIP5, carbon-cycle, climate change

Supplementary material for this article is available online

OPEN ACCESS

RECEIVED
15 January 2015

REVISED
26 April 2015

ACCEPTED FOR PUBLICATION
29 April 2015

PUBLISHED
22 May 2015

Abstract

Terrestrial ecosystems currently sequester about one third of anthropogenic CO_2 emissions each year, an important ecosystem service that dampens climate change. The future fate of this net uptake of CO_2 by land based ecosystems is highly uncertain. Most ecosystem models used to predict the future terrestrial carbon cycle share a common architecture, whereby carbon that enters the system as net primary production (NPP) is distributed to plant compartments, transferred to litter and soil through vegetation turnover and then re-emitted to the atmosphere in conjunction with soil decomposition. However, while all models represent the processes of NPP and soil decomposition, they vary greatly in their representations of vegetation turnover and the associated processes governing mortality, disturbance and biome shifts. Here we used a detailed second generation dynamic global vegetation model with advanced representation of vegetation growth and mortality, and the associated turnover. We apply an emulator that describes the carbon flows and pools exactly as in simulations with the full model. The emulator simulates ecosystem dynamics in response to 13 different climate or Earth system model simulations from the Coupled Model Intercomparison Project Phase 5 ensemble under RCP8.5 radiative forcing. By exchanging carbon cycle processes between these 13 simulations we quantified the relative roles of three main driving processes of the carbon cycle; (I) NPP, (II) vegetation dynamics and turnover and (III) soil decomposition, in terms of their contribution to future carbon (C) uptake uncertainties among the ensemble of climate change scenarios. We found that NPP, vegetation turnover (including structural shifts, wild fires and mortality) and soil decomposition rates explained 49%, 17% and 33%, respectively, of uncertainties in modelled global C-uptake. Uncertainty due to vegetation turnover was further partitioned into stand-clearing disturbances (16%), wild fires (0%), stand dynamics (7%), reproduction (10%) and biome shifts (67%) globally. We conclude that while NPP and soil decomposition rates jointly account for 83% of future climate induced C-uptake uncertainties, vegetation turnover and structure, dominated by biome shifts, represent a significant fraction globally and regionally (tropical forests: 40%), strongly motivating their representation and analysis in future C-cycle studies.

1. Introduction

Since the 1960s terrestrial ecosystems have sequestered about one third of anthropogenic CO_2 emissions (Le Quéré *et al* 2014), providing an important ecosystem service in mitigating climate change. The future evolution of this land sink of CO_2 is uncertain. In part, the uncertainty originates from

differences in the climate projections as identified in a number of studies that forced specific ecosystem models with ensembles of climate outputs from general circulation models (GCMs) or earth system models (ESMs) (Berthelot *et al* 2005, Schaphoff *et al* 2006, Scholze *et al* 2006, Ahlström *et al* 2012b, Ahlström *et al* 2013). Further uncertainty in projections arises from the different representations of land ecosystems and the carbon cycle processes in different ecosystem models, as illustrated in studies forcing ensembles of ecosystem models with common climate information (Cramer *et al* 2001, McGuire *et al* 2001, Friend *et al* 2013).

The terrestrial carbon cycle can be expressed conceptually quite simply, as the change of the total amount of carbon in an ecosystem (C_{eco}) is determined by the balance between net uptake and release of carbon (equation (1)).

$$\frac{dC_{eco}}{dt} = NPP - \tau C_{eco}, \quad (1)$$

where net primary production (NPP) denotes the total ecosystem carbon influx through NPP and τ is the turnover rate (inverse residence time) of carbon expressed as the fraction of C_{eco} leaving the system over time dt. Most ecosystem models adopt a pool-based extension of this basic model, where the accrued NPP is first allocated to plant compartments, leading to growth. The processes governing turnover differ between compartments. Leaf carbon turnover for instance depends chiefly on the plant's phenology, e.g. deciduous or evergreen. By contrast, turnover of stems and branches in woody perennial plants is regulated through stand dynamics such as establishment, growth and self-thinning, age-related mortality and disturbances such as wild fires. Through vegetation turnover carbon is transferred to litter and soil carbon pools, where it is returned to the atmosphere through decomposition by soil microbes or by wild fires. Environmental regulation differs for different turnover processes, leading to large uncertainties as the response of the individual processes to climate change or changes in atmospheric CO_2 is not well known, and this is reflected in different process representations in different models (Friend *et al* 2013, Carvalhais *et al* 2014). What may be more important is that processes describing vegetation dynamics, accounting for mortality and disturbance as well as biome shifts, have to date rarely been included in global models used to predict future carbon uptake (Wolf *et al* 2011).

Here we adopted a detailed individual-based ecosystem model with advanced representation of vegetation dynamics to investigate the relative role of different aspects of ecosystem dynamics governing carbon balance (hereinafter referred to as ecosystem processes) for future carbon uptake uncertainties at global and regional scales. We applied the traceability framework (Xia *et al* 2013) to construct an emulator of future steady state carbon pools under an ensemble of climate change projections. This method allowed us to reduce a complex model to its main processes while preserving its structure. That way, we could exchange carbon-cycle processes between emulator representations of model simulations and investigate their relative roles for the future terrestrial uptake of CO_2 under different projections of climate change. We focused on three main carbon cycle processes: (I) NPP, (II) vegetation turnover and structure, and (III) environmental scalars affecting soil decomposition rates. We further split vegetation turnover and structure into (1) non-fire disturbance represented by a stochastic clearing of all standing vegetation in a vegetation patch, (2) fire disturbance emitting carbon directly to the atmosphere as well as inducing mortality, (3) stand dynamics including mortality related to competition for resources between age-groups of plant individuals, and (4) turnover related to demographic processes in conjunction with simulated changes in the distribution of plant functional types (PFTs) (vegetation structure), commonly termed biome shifts, to understand their individual roles in terrestrial carbon cycle uncertainties.

2. Methods

Below we first introduce the full model our study is based on (section 2.1) and the performed simulations (2.2). In section 2.3 we describe the traceability framework and how it has been implemented as an emulator to trace ecosystem processes of the full model. We explain the experimental design in section 2.4, including a step-by-step example of how the relative contributions of ecosystem processes to overall simulated dynamics are found. Section 2.5 describes the definition of land cover classes used in the regional assessment.

2.1. LPJ-GUESS

We employed LPJ-GUESS, a global dynamic vegetation-ecosystem model based on a detailed, individual- and patch-based representation of vegetation structure, demography and resource competition (Smith *et al* 2001). Vegetation is represented as PFTs (PFTs; 11 in this study; Ahlström *et al* 2012a) distinguished by bioclimatic limits, growth form (trees versus herbaceous plants), phenology (evergreen, summergreen and raingreen), life history strategy (shade tolerant or intolerant) and photosynthetic pathway (C_3 or C_4). We used the model in cohort mode, in which individual plants are grouped into age classes of PFTs (cohorts) within a number of replicate patches (10 in this study) to account for stochastic variability across each grid cell. The detailed representation of plant size structure and demographics may improve simulations of large scale fluxes and carbon stocks (Purves and Pacala 2008, Fisher *et al* 2010, Wolf *et al* 2011, Haverd *et al* 2014, Brienen *et al* 2015).

Population dynamics are represented by competition between cohorts for light, water and space.

Table 1. CMIP5 models and modelling groups.

Modelling center (or group)	Institute ID	Model name
Canadian Centre for Climate Modelling and Analysis	CCCMA	CanESM2
National Center for Atmospheric Research	NCAR	CCSM4
Commonwealth Scientific and Industrial Research Organization in collaboration with Queensland Climate Change Centre of Excellence	CSIRO-QCCCE	CSIRO-Mk3.6.0
EC-EARTH consortium	EC-EARTH	EC-EARTH
NOAA Geophysical Fluid Dynamics Laboratory	NOAA GFDL	GFDL-ESM2M
NASA Goddard Institute for Space Studies	NASA GISS	GISS-E2-R
Met Office Hadley Centre	MOHC	HadGEM2-ES
Institute for Numerical Mathematics	INM	INM-CM4
Institut Pierre-Simon Laplace	IPSL	IPSL-CM5A-LR
Atmosphere and Ocean Research Institute (The University of Tokyo), National Institute for Environmental Studies, and Japan Agency for Marine-Earth Science and Technology	MIROC	MIROC5
Max Planck Institute for Meteorology	MPI-M	MPI-ESM-LR
Meteorological Research Institute	MRI	MRI-CGCM3
Norwegian Climate Centre	NCC	NorESM1-M

Mortality occurs following low or negative growth efficiency, age, or due to a change in climate to conditions beyond the PFT's bioclimatic limits. Disturbance are represented by a stand-clearing stochastic event with an expected return time of 100 years and wild fires, modelled prognostically based on temperature, current fuel load and moisture (Thonicke *et al* 2001). A detailed description of LPJ-GUESS is given in Smith *et al* (2001).

2.2. Simulations

Transient and steady-state simulations were performed of the response of the terrestrial biosphere to climate projections and atmospheric CO_2 concentrations under the RCP 8.5 representative concentration pathway (Riahi *et al* 2007). We used climate outputs from an ensemble of 13 CO_2 concentration-driven GCMs and ESMs (table 1) contributing to the Coupled Model Intercomparison Project Phase 5 (CMIP5) (Taylor *et al* 2011). We adopted a bias correction described in Ahlström *et al* (2012b) where climate fields from each projection were corrected to match CRU TS3.10 (Harris *et al* 2014) 1961–1990 monthly climatologies.

In the steady-state simulations, the model was forced directly to steady state at year 2085 by recycling climate drivers over 2071–2100 for 510 years. The recycled climate data were detrended to remove trends that may cause abrupt changes in the forcing between recycled periods which can lead to die-back and recovery cycles of vegetation, preventing convergence to steady state. During initialization, soil C influx and decomposition rates were used to analytically find the steady state soil carbon pool sizes (steady state C pool = C influx/decomposition rate) (Sitch *et al* 2003). Time invariant land use fractions followed the RCP 8.5 (Hurtt *et al* 2011) for the year 2085, and atmospheric CO_2 levels were fixed at 801 ppm (RCP 8.5 2085 level).

Transient simulations were similar but employed time-variant climate, CO_2 concentrations and land use from the same set of projections. The model was first initialized to steady state for pre-industrial conditions following the standardized protocol described in Ahlström *et al* (2012b).

2.3. Traceability framework

The traceability framework was developed to fulfil the need for a transparent method to identify sources of uncertainties stemming from process representations in complex land models (Xia *et al* 2013). The framework decomposes the target model into traceable components based on the recognition that all global land carbon cycle models share some common yet mutually independent core processes (Luo *et al* 2003, Luo and Weng, 2011, Luo *et al* 2014). The traceability framework preserves the structure of the full model it replaces, tracing carbon from initial uptake (NPP) through plant and soil carbon pools until it leaves the system and is returned to the atmosphere. The framework extends the basic model described in equation (1), where the change in a carbon pool is described as the balance of input and output, by describing the individual carbon pools and flows as it is implemented in models and realized in simulations (equation (2).

$$\frac{dX}{dt} = B\mathrm{NPP} - \xi ACX, \tag{2}$$

where X is the size of carbon pools, B is the partitioning fractions of NPP into plant compartments, ξ stands for a number of environmental scalars, A denotes carbon pool transfer fractions, and C are the prescribed baseline turnover rates.

Setting the change in carbon pools to zero ($dX/dt = 0$) and rearranging equation (2) allows analytical solution of steady state carbon pools (equation (3).

$$X_{ss} = \frac{B_{ss}\mathrm{NPP}_{ss}}{\xi_{ss}A_{ss}C_{ss}}, \tag{3}$$

where ss denotes steady state values.

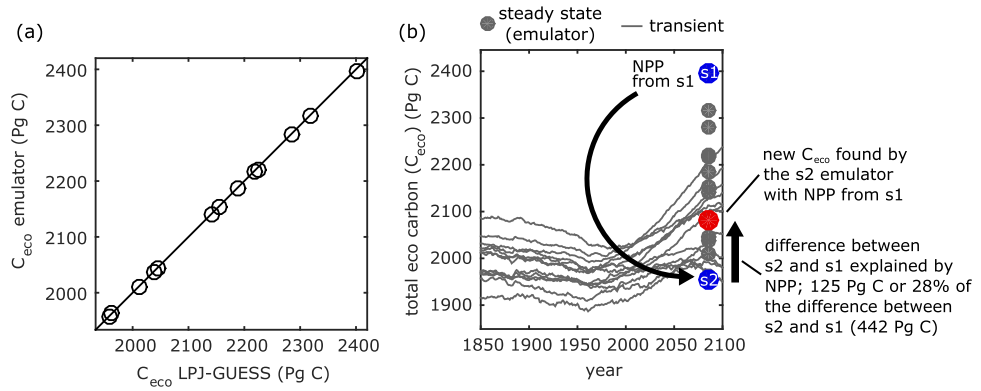

Figure 1. Emulator performance and example of experimental design. (a) Comparison between global C_{eco} at steady state as simulated by LPJ-GUESS and emulator (equation (3)) solution of global C_{eco} at steady state for the 13 simulations and emulator solutions. The small deviations from the 1:1 relationship (black line) are mainly due to the internal variability in LPJ-GUESS where true steady state is never reached, in contrast to the emulator, which solves the steady state conditions analytically. (b) Illustration of experimental design using data from figure 2(a). Grey curves are time trajectories of C_{eco} from transient simulations with LPJ-GUESS; circles denote corresponding emulator-computed steady state values of C_{eco}. Simulation s1 in this example shows a steady state C_{eco} (2398 Pg C) that is larger than simulation s2 C_{eco} (1956 Pg C). When replacing the lower NPP from simulation s2 with the larger NPP from simulation s1 in the emulator representation of s2 a new, larger, C_{eco} was computed by the emulator: 2081 Pg C. The part of the difference between simulation s2 and s1 explainable by NPP is therefore 2081−1956 = 125 Pg C, which corresponds to 28% of the total difference between the simulation pair (442 Pg C). The same procedure is repeated for processes (I–III) and for all pairs of simulations. In figure 2(b), the example described above is plotted as a green diamond, with *x*-axis value of 442 and *y*-axis value of 125.

Here we applied the traceability framework to a dynamic vegetation model. As this traceability analysis can only be applied to steady state simulations, we had to get the steady-state solutions of the dynamic vegetation model. Due to vegetation dynamics occurring in the model in each simulation year, combined with varying climate, the model never reaches true steady state. Instead, we calculated parameters from the average of the last 60 years of the 510 years simulation.

The dynamic vegetation in LPJ-GUESS requires some adjustments to be made to the implementation of the traceability framework. Following equations (2) and (3) above, the turnover rate of carbon pools depends on environmental scalars (e.g. temperature and soil moisture) and pre-set baseline turnover times. Although in LPJ-GUESS PFTs differ in their expected maximum age and leaf turnover, the actually simulated (realized) vegetation turnover also depends on mortality associated with competition between plants for resources and space, a range of disturbances, as well as the dynamic PFT composition. As a result of these dynamics, the realized vegetation turnover cannot be predicted from preset model parameters and climate alone and the realized turnover cannot readily be decomposed into environmental and stand structural components. Therefore, here we set the environmental scalars for vegetation pools to 1 and calculate turnover from the respective fluxes and pools (equation (4)).

$$\xi_{\mathrm{veg}_i} C_i = \frac{F_{\mathrm{tot}_i}}{X_{\mathrm{ss}_i}}, \qquad (4)$$

where the environmental scalar ξ_{veg} is 1, C is the turnover rate, F_{tot} denotes the sum of all fluxes from vegetation pool i and X_{ss} is the steady state carbon pool size of vegetation pool i. C is therefore not a baseline turnover for vegetation pools, but rather the realized turnover rate.

Soil and litter carbon pools follow the standard implementation (Xia *et al* 2013), where the turnover rate is decomposed into an environmental scalar and baseline turnover rates representing different chemical and structural composition of the carbon in litter and slow and fast soil pools (figure S1).

2.4. Experimental design

To investigate the role of three main carbon cycle processes we exchanged traceability framework components (carbon cycle processes) pairwise among the 13 simulations and recorded the size of the resulting carbon pools and how much the difference in C-storage between a pair of simulations changes per exchanged component. This method utilizes the traceability framework to compute an emulator of steady state carbon pool sizes (equation (3)). Solving equation (3) for any given simulation results in nearly identical carbon pool sizes compared to steady state outputs from LPJ-GUESS, any difference being accounted for by stochastic dynamics in LPJ-GUESS that inhibit exact adherence to steady state (Figure 1(a)).

Three processes and combination of processes were exchanged, (I) NPP, (II) vegetation turnover, NPP partitioning, and vegetation transfer fractions (C, B and A for vegetation pools), and (III) soil and litter environmental scalars (decomposition rates), between each of the 156 (13×12) unique two-way combination of the 13 simulations.

An illustrative example of the uncertainty partitioning approach is shown in figure 1(b). In order to

find the difference in the global total terrestrial carbon pool (C_{eco}) explained by the difference in NPP between the simulation resulting in the largest C_{eco} (simulation s1; 2398 Pg C) and the simulation resulting in the lowest C_{eco} (simulation s2; 1956 Pg C), we first find the C_{eco} resulting from a substitution of NPP from simulation s1 (63.9 Pg C) to the emulator representing simulation s2 (60.4 Pg C):

$$X_{ss} = \frac{B_{ss_{S2}} \mathrm{NPP}_{ss_{S2}}}{\xi_{ss_{S2}} A_{ss_{S2}} C_{ss_{S2}}}, \quad (5)$$

where the new C_{eco} is the sum of X_{ss} over all carbon pools (ΣX_{ss}: 2081 Pg C) with NPP from simulation s1. Next we calculate the difference between the new, modified, s2 C_{eco} with NPP from simulation s1 and the original C_{eco} of simulation s2: 2081 −1956 = 125 Pg C. The relative difference explained by modelled NPP under the alternative forcings of s1 and s2 is therefore 28% (absolute difference explained/difference; 125/(2398−1956) = 0.2828) (figure 1(b)).

This procedure was repeated for all pairs of simulations ($n = 156$; see above) and for each process (I–III), making 468 (156 simulation pairs × 3 exchanged processes) emulator realizations altogether. Due to differences in the spatial and temporal characteristic of the forcing climate and the non-linear response to the forcing, the fraction explained by processes I–III differs between unique combinations of simulations. Therefore we find the overall—ensemble mean—fraction explained by each carbon cycle process by employing regression analysis:

$$Y = \beta X + \varepsilon, \quad (6)$$

where Y is the difference explained by a carbon cycle process ($n = 156$), β represents the ensemble overall fraction explained by a carbon cycle process, X is the difference in carbon pool size between a given pair of simulations and ε is the error term.

We focused our analysis on three pools of carbon: total ecosystem carbon, C_{eco}; carbon in vegetation pools (leaf, heartwood, sapwood and roots), C_{veg}; and carbon residing in soil and litter pools, $C_{soil+litter}$, where the latter two are found by summing X_{ss} over vegetation and soil and litter pools respectively.

2.4.1. Partitioning of vegetation turnover

We further investigated the relative role of different types of vegetation turnover by discriminating the turnover due to a range of processes and disturbance types. Five such classes of processes were distinguished: (1) turnover due to patch-clearing, non-fire disturbance; (2) disturbance due to wild fires (instantaneous emissions due to burning of biomass as well as mortality following fire events); (3) stand dynamics from mortality caused by competition for resources and space among age cohorts of co-occurring plant individuals from the same or different PFTs; and (4) turnover due to biome shifts, encapsulated by the PFT composition, which affects vegetation demography and associated expected residence time of biomass carbon. We also included in our analysis (5) the fraction of NPP that is partitioned to the reproduction pool, prescribed at 10% of NPP. The reproduction pool is emitted to the atmosphere every year and represents carbon costs associated with reproduction, such as the production of flowers, seeds and pheromones.

The roles of different types of vegetation turnover and structural components were found by comparing the total vegetation turnover of each simulation (sum of all fluxes from vegetation pools, including fire emissions to the atmosphere and litter fall, g C) to the vegetation turnover due to each of the four turnover and structural component types (g C). We therefore did not exchange turnover and structural components between simulations, but rather analyze what processes or components cause the difference in turnover between simulations, which in turn explains a fraction of overall carbon pool uncertainty as described by the analysis above.

2.5. Definition of land cover classes

We evaluated the contribution of individual processes to carbon pool patterns globally and differentiated into six broad land-cover classes, characteristic of major climate zones or global regions. The land-cover class definitions are based on the MODIS land cover classification (MCD12C1, type3, (Friedl *et al* 2010)) from satellite-borne remote sensing remapped using a majority filter to a spatial resolution of 0.5 × 0.5°, thus representing the dominant land cover in each 0.5 × 0.5° grid cell. The land-cover classes distinguished were: tropical forests, extra-tropical temperate and boreal forests, semi-arid savannah and shrublands, tundra and cold shrublands, grasslands and land under agriculture (crops), and areas classified as barren (sparsely vegetated). The MODIS category 'forest' was split into tropical forest and extra-tropical forest using the Köppen–Geiger climate classification system (Köppen 1936), where tropical forests were distinguished by the A climate group (mean temperature of any month over 1982–2011, never falling below 18 °C). Semi-arid savannas and shrublands were separated from tundra and cold shrublands at latitude 45°N. We averaged and area-weighted the outputs of the model for each of the seven analyzed regions (global and six landcover classes) before calculating traceability framework parameters. Using fixed, present-day land cover classes instead of using the model-predicted future land cover classes allowed us to accurately trace uncertainties related to biome shifts.

3. Results

3.1. Global analysis

Comparing steady-state C_{eco} (total ecosystem carbon content, comprising the sum of vegetation, soil and

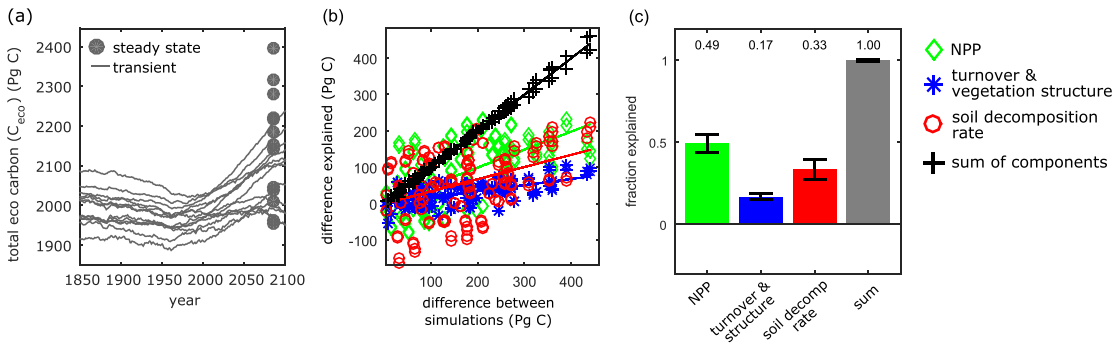

Figure 2. Global partitioning of steady state C_{eco} uncertainties. (a) Comparison of transient simulations and steady state total ecosystem carbon. (b) Relationships between differences in global C_{eco} between pairs of simulations and C_{eco} explained by three main carbon cycle processes defined as the decrease in C_{eco} difference between simulation pairs when exchanging a given process. Black crosses depict the sum of the difference explained by the three processes. (c) Fractions of global C_{eco} explained by carbon cycle processes. The fractions were defined as the slopes of the regression lines in panel (b) (equation (6)). Error bars represent 5–95% confidence intervals of the regression coefficients.

litter carbon) and transient simulations at year 2085 showed that the spread (i.e. the distribution of C_{eco} in the ensemble of simulations, ranging from 1956 to 2398 Pg C), between simulations at steady state is about twice the spread seen in transient simulations (figure 2(a)), with similar relative differences between simulations. These differences between transient and steady-state conditions are in part due to successional responses to environmental- and land use change, and in part due to slow overturning mainly in the soil carbon pools, which both operate on long time-scales. Comparison of differences in C_{eco} and the difference explained by the three processes NPP, turnover and structure, and soil decomposition rate showed a large spread between pairs of simulations (figure 2(b)). The differences explained by individual components have different slopes (equation (6)) which may be interpreted as the fraction of the ensemble spread explained by that component (figure 2(b)). On this basis, differences in NPP between simulations explained 49% of the spread in C_{eco} that was observed within the climate change ensemble at 2085 (figure 2(c)). Vegetation turnover and structure explained 17%, while soil decomposition rate explained the remaining 33%. Jointly, the three fractions summed to 1, indicating that the three components together explained the entire ensemble spread in steady state C_{eco} at 2085.

When repeating the analysis for C_{veg}, NPP explained 61% and turnover 39% of global C_{veg} spread (figures 3(a)–(c)). Since soil decomposition does not affect vegetation processes in LPJ-GUESS (and in the emulator), soil moisture and temperature scalars explained 0% of C_{veg} spread. For soil and litter carbon ($C_{soil+litter}$), soil moisture and temperature regulation of decomposition were more important (60%) than differences in the input of carbon that is dependent on NPP (36%) and vegetation turnover and structure (5%) (figures 3(d)–(f)).

3.1.1. Partitioning of global vegetation turnover

The partitioning of vegetation turnover showed that biome shifts, as encapsulated by differences in PFT composition between the simulations, explained 67% of the observed differences between simulations: non-fire disturbance explained 16%, stand dynamics 7% and turnover due to reproduction 10%. Fire disturbance played no role (0% explained) in governing global differences in vegetation turnover among simulations (figure 4).

3.2. Regional analysis

Repeating the analysis of C_{eco} for five global land-cover classes (based on a MODIS land cover classification for year 2000; see section 2.5) showed large regional differences (figure 5). In tropical forests, where a relatively large fraction of C_{eco} resides in vegetation pools, NPP and vegetation turnover dominated, explaining 56% and 40%, respectively, of the observed spread in C_{eco} between future simulations. By contrast, in tundra and arctic shrubland, where a larger fraction of C resides below ground, uncertainties introduced by the different climate projections are mainly explained by climatic control of soil decomposition (80%) and only 20% by NPP. In grasslands and croplands, NPP (48%) explained a similar fraction to the soil decomposition scalars (45%) and only a small fraction (6%) was due to vegetation turnover and structure. C_{eco} in semi-arid ecosystems was more responsive to variation in NPP (62%) than extra-tropical forests (34%).

3.2.1. Partitioning of regional vegetation turnover

Biome shifts and associated differences in PFT distribution between simulations explained a large fraction in all land-cover classes (figure 5). Fire disturbance was most important in semi-arid ecosystems (15%) and least important in tropical forest (−12%). The negative contribution of wild fires to future C_{eco} uncertainties implies that differences in fire emissions and fire

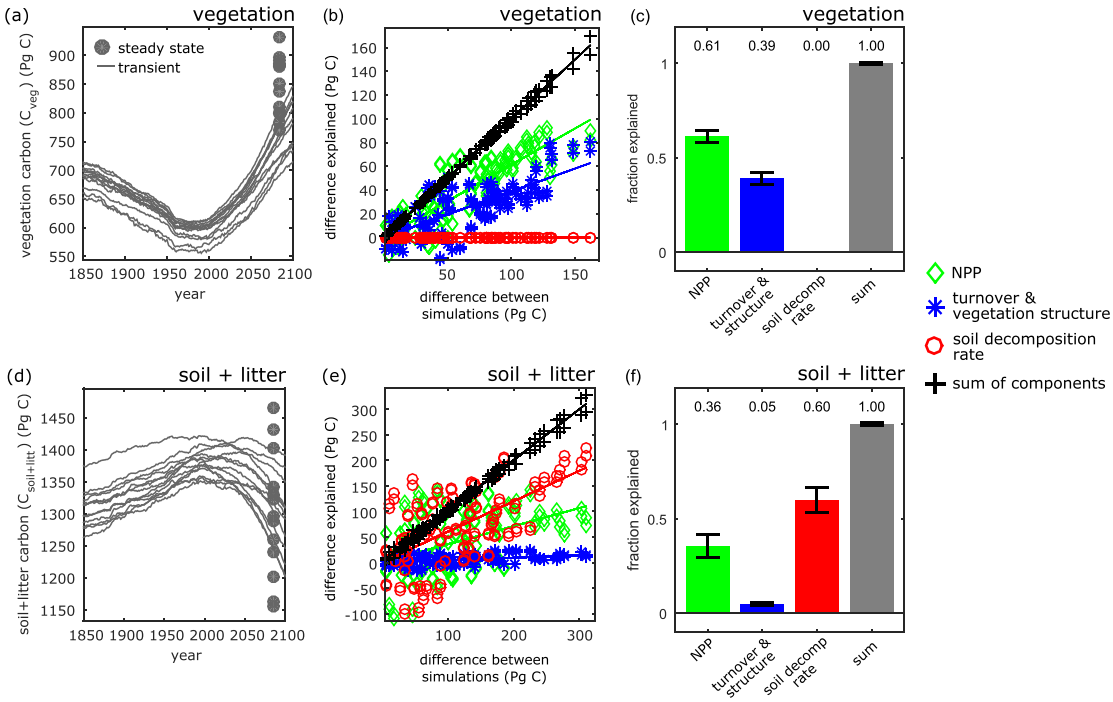

Figure 3. Global partitioning of steady state C_{veg} and $C_{soil+litter}$ uncertainties. (a) Comparison of transient simulations and steady state vegetation carbon. (b) Relationships between differences in global C_{veg} between pairs of simulations and C_{veg} explained by three main carbon cycle processes defined as the decrease in C_{veg} difference between pairs when exchanging a given component. Black crosses depict the sum of the difference explained by the three processes. (c) Fractions of global C_{veg} explained by carbon cycle components, corresponding to slopes of the regression lines in panel (b). Error bars represent 5–95% confidence intervals of the regression coefficients. Panels (e)–(f) show the corresponding results for soil and litter carbon uncertainties.

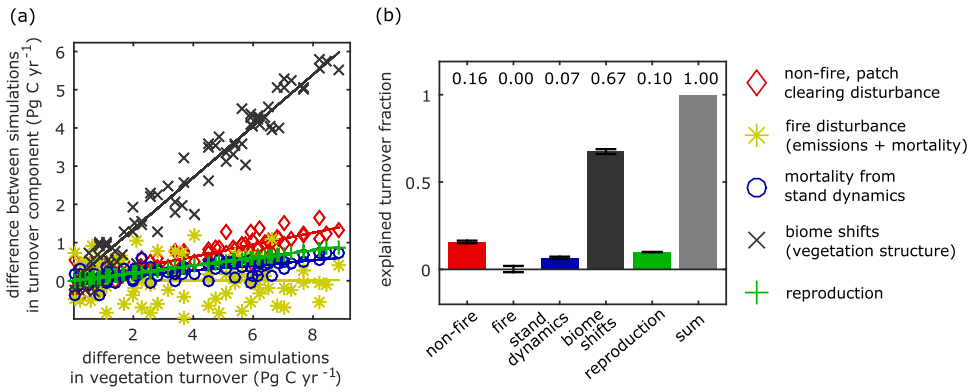

Figure 4. Global partitioning of vegetation turnover into turnover components and processes. (a) Difference in total vegetation turnover between simulation pairs and difference in turnover components between pairs. Slope corresponds to the importance of a given turnover component in explaining total turnover spread. (b) Vegetation turnover spread explained by components. The fractions were defined as the slopes of the regression lines in panel (a). Error bars represent 5–95% confidence intervals of the regression coefficients.

induced mortality decrease the overall spread between the simulations, thus contributing negatively to the uncertainty. In other words, in extra-tropical forest, grasslands and crops, and tropical forest, fire emissions and mortality due to fires are generally larger in high C uptake simulations than in low C uptake simulations. The occurrence of both positive (increasing spread) and negative regional fire contributions (decreasing spread) to C_{eco} uncertainties is the explanation for why fires explain 0% of global C_{eco} uncertainties (figure 2).

Stand dynamics are linked to C-cycle turnover due to competition for resources between plant age cohorts, an important factor in closed-canopy forests. In LPJ-GUESS, non-fire disturbance has a prescribed expected return time of 100 years. The background, non-fire effects varied between simulations and regions mainly because of the dependency on the amount of carbon in vegetation, but also because of interactions with the frequency of other turnover components and the decomposition of the resulting

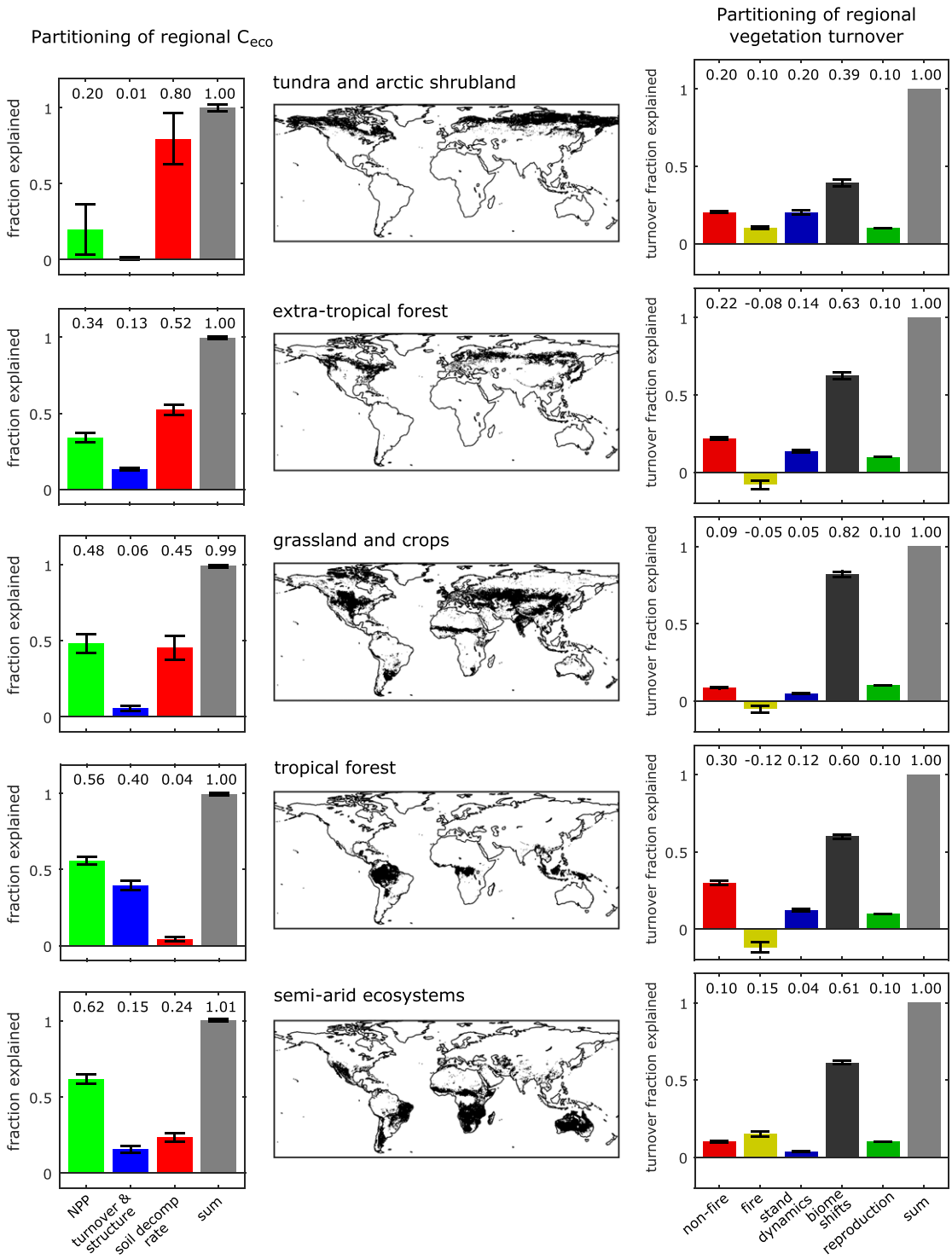

Figure 5. Regional partitioning of C_{eco} uncertainties into carbon cycle components and regional partitioning of vegetation turnover processes. From top to bottom, rows show land cover classes derived from the MODIS MCD12C1 Type 3 land cover product (further details in section 2.5). From left to right, columns show; partitioning of C_{eco} into carbon cycle components and processes, definition of land cover class, and partitioning of vegetation turnover.

litter. In our simulations we accounted for reproduction costs by assigning 10% of NPP to a separate reproduction pool, with a residence time of one year. Reproduction accounted for a fixed fraction of explained turnover differences in all regions. This is because we evaluate steady state conditions where NPP, the influx of carbon to vegetation pools, must be equal to the sum of all fluxes leaving the vegetation pool, and a fixed fraction of NPP is therefore also a fixed fraction of total turnover.

4. Discussion

By applying the traceability framework to emulate a full process-based global ecosystem model, we have

illustrated how climate-induced future carbon cycle uncertainties can be partitioned into the main ecosystem processes underlying observed variability within an ensemble under steady state conditions. The resulting fractions explained by the three processes almost exactly sum to unity globally (figures 2 and 3) and regionally (figure 5), indicating that the method used accounts almost perfectly for climate model-induced uncertainties among simulated ecosystem processes. A shortcoming of our approach is that by exchanging individual carbon cycle processes, feedbacks that exist between ecosystem processes are decoupled. Examples of such omitted feedbacks include the interdependence of photosynthesis (as a major component of NPP) on transpiration, the latter affecting soil moisture, which in turn will affect NPP. The effects of disturbances on biomass turnover and NPP are another example. Further, our methodology decouples the tight interplay between NPP and stand structure and demographics also seen in observations (Michaletz *et al* 2014). Given the dependency of NPP on stand age and demographics, it is likely that also some of the differences in NPP between simulations results from vegetation dynamics and the resulting stand structure. However, this decoupling allowed us to characterize the isolated impacts of different processes providing important information on their impacts on climate induced future carbon cycle uncertainties.

Our results represent a first attempt to partition climate model-induced terrestrial carbon-cycle uncertainties into individual ecosystem processes, an important step beyond previous studies (Berthelot *et al* 2005, Schaphoff *et al* 2006, Ahlström *et al* 2012b, Ahlström *et al* 2013). This helps to identify the most important mechanisms contributing to simulation variability, providing guidance to modellers faced with the choice of which processes to focus on in revising and improving their models, while highlighting the types of observational data most needed to validate models and fill process knowledge gaps. The method applied allows partitioning of uncertainties in steady state and results may therefore be expected to differ from uncertainties in transient simulations. However, the amount of carbon stored in different ecosystem compartments at steady state represents useful information on how the ecosystem will respond to climate change in the long term, and may be seen as the state towards which a transient simulation is heading.

The contribution from individual carbon-cycle processes to the total simulated variability in C_{eco} is a result of uncertainties in climate model forcing as well as the simulated ecosystem response to such forcing. As an example, the environmental control of soil decomposition was found to play a large role governing uncertainty in tundra and cold ecosystems, in part due to the relatively large amount of carbon stored in soils in these regions but also due to a large spread among projections in the magnitude of warming, especially during winter when photosynthesis is inactive (Ahlström *et al* 2012b).

Wolf *et al* (2011) demonstrated that global land surface models lacking detailed vegetation dynamics and stand demography fail to reproduce observed biomass and allometric patterns, including the associated turnover. The model applied here, LPJ-GUESS, has such a detailed representation of vegetation dynamics, and has been shown to reproduce observed allometric relationships seen in global forest inventories, and reflecting the coupling between forest structure and functioning, more faithfully than most land surface models (Smith *et al* 2014). Although climate impact on NPP emerges as the most important overall process for C_{eco} uncertainties in our analysis, vegetation dynamics and especially different biome distributions between simulations was an important factor (globally: 17%). Regionally, the importance of vegetation dynamics in explaining variability in C_{eco} ranged from 1% for tundra and arctic shrubland to 40% in tropical forest (figure 5).

While a recent modelling study concluded that the likelihood of net carbon losses in tropical forests under future climate change is low (Huntingford *et al* 2013), a recent forest inventory study suggests that increasing mortality together with a stagnation in productivity has led to a decline in vegetation carbon in the Amazon over the last two decades (Brienen *et al* 2015). The analysis of the present study indicates that the uncertainty of climate change impacts on tropical forests future carbon storage is mediated mainly through productivity (NPP; 56%) and vegetation dynamics (vegetation turnover; 40%), where the simulated response depends on the characteristics of future climate change over tropical forests, including changes in mean climate variables, their co-variation, as well as variations on a multitude of time scales. Although none of our simulations resulted in a pronounced dieback of tropical forest vegetation (figure S2), the large uncertainty seen in future tropical forest C-storage due to vegetation dynamics suggests that adequate representations of vegetation dynamic processes, including mortality and disturbances, in models may be a key to producing accurate projections of climate change impacts on carbon storage for the wet tropics.

The relative roles of ecosystem processes across regions co-vary with general ecosystem properties; ecosystems where the majority of carbon resides in soil and litter pools are more responsive to soil decomposition rates, determined by soil temperature and moisture, while ecosystems dominated by above ground carbon stocks, tend to be more responsive to changes in production, vegetation turnover and structure. Although the general patterns found in this study may not be unexpected, they represent a first quantification of the relative roles of carbon cycle processes for future C-uptake uncertainties. In conclusion, our results suggest that vegetation dynamics merit attention in future model development and studies

analyzing the future terrestrial carbon cycle and its feedbacks to global climate change.

Acknowledgments

Anders Ahlström acknowledges support from the Swedish Foundation for Strategic Environmental Research (Mistra) through the Mistra-SWECIA programme, The Royal Physiographic Society in Lund (Birgit and Hellmuth Hertz' Foundation) and the Swedish Research Council (grant no. 637-2014-6895). Almut Arneth acknowledges support from the Helmholtz Foundation through the ATMO programme and through its Integration and Networking Fund, and from the EU FP7 project LUC4C (grant 603542). Benjamin Smith acknowledges funding as an OCE Distinguished Visiting Scientist to the CSIRO Ocean and Atmosphere Flagship, Canberra. The study is a contribution to the Lund University Centre of Excellence LUCCI and the strategic research areas Modelling the Regional and Global Earth System (MERGE) and Biodiversity and Ecosystem Services in a Changing Climate (BECC). We acknowledge the World Climate Research Programme's Working Group on Coupled Modelling, which is responsible for CMIP, and we thank the climate modelling groups (listed in table 1 of this paper) for producing and making available their model output. For CMIP the US Department of Energy's Program for Climate Model Diagnosis and Intercomparison provides coordinating support and led development of software infrastructure in partnership with the Global Organization for Earth System Science Portals. The MODIS MOD12C1 land cover product was obtained through the online Data Pool at the NASA Land Processes Distributed Active Archive Center (LP DAAC), USGS/Earth Resources Observation and Science (EROS) Center, Sioux Falls, South Dakota (https://lpdaac.usgs.gov/data_access).

References

Ahlström A, Miller P A and Smith B 2012a Too early to infer a global NPP decline since 2000 *Geophys. Res. Lett.* **39** L15403

Ahlström A, Schurgers G, Arneth A and Smith B 2012b Robustness and uncertainty in terrestrial ecosystem carbon response to CMIP5 climate change projections *Environ. Res. Lett.* **7** 044008

Ahlström A, Smith B, Lindström J, Rummukainen M and Uvo C B 2013 GCM characteristics explain the majority of uncertainty in projected 21st century terrestrial ecosystem carbon balance *Biogeosciences* **10** 1517–28

Berthelot M, Friedlingstein P, Ciais P, Dufresne J-L and Monfray P 2005 How uncertainties in future climate change predictions translate into future terrestrial carbon fluxes *Glob. Change Biol.* **11** 959–70

Brienen R J W *et al* 2015 Long-term decline of the Amazon carbon sink *Nature* **519** 344–8

Carvalhais N *et al* 2014 Global covariation of carbon turnover times with climate in terrestrial ecosystems *Nature* **514** 213–7

Cramer W *et al* 2001 Global response of terrestrial ecosystem structure and function to CO_2 and climate change: results from six dynamic global vegetation models *Glob. Change Biol.* **7** 357–73

Fisher R, Mcdowell N, Purves D, Moorcroft P, Sitch S, Cox P, Huntingford C, Meir P and Ian Woodward F 2010 Assessing uncertainties in a second-generation dynamic vegetation model caused by ecological scale limitations *New Phytologist* **187** 666–81

Friedl M A, Sulla-Menashe D, Tan B, Schneider A, Ramankutty N, Sibley A and Huang X 2010 MODIS Collection 5 global land cover: algorithm refinements and characterization of new datasets *Remote Sens. Environ.* **114** 168–82

Friend A D *et al* 2013 Carbon residence time dominates uncertainty in terrestrial vegetation responses to future climate and atmospheric CO_2 *Proc. Natl. Acad. Sci. USA* **111** 3280–5

Harris I, Jones P D, Osborn T J and Lister D H 2014 Updated high-resolution grids of monthly climatic observations—the CRU TS3.10 Dataset *Int. J. Climatol.* **34** 623–42

Haverd V, Smith B, Nieradzik L P and Briggs P R 2014 A stand-alone tree demography and landscape structure module for Earth system models: integration with inventory data from temperate and boreal forests *Biogeosciences* **11** 4039–55

Huntingford C *et al* 2013 Simulated resilience of tropical rainforests to CO_2-induced climate change *Nat. Geosci.* **6** 268–73

Hurtt G *et al* 2011 Harmonization of land-use scenarios for the period 1500–2100: 600 years of global gridded annual land-use transitions, wood harvest, and resulting secondary lands *Clim. Change* **109** 117–61

Köppen W 1936 Das geographische System der Klimate ed W Köppen and R Geiger *Handbuch der Klimatologie.* (Berlin: Bd. Gebr Borntröger I)

Le Quéré C *et al* 2014 Global carbon budget 2013 *Earth Syst. Sci. Data* **6** 235–63

Luo Y, Keenan T F and Smith M 2014 Predictability of the terrestrial carbon cycle *Glob. Change Biol.* doi:10.1111/gcb.12766

Luo Y and Weng E 2011 Dynamic disequilibrium of the terrestrial carbon cycle under global change *Trends Ecol. Evol.* **26** 96–104

Luo Y, White L W, Canadell J G, Delucia E H, Ellsworth D S, Finzi A, Lichter J and Schlesinger W H 2003 Sustainability of terrestrial carbon sequestration: a case study in Duke Forest with inversion approach *Glob. Biogeochem. Cycles* **17** 1021

Mcguire A D *et al* 2001 Carbon balance of the terrestrial biosphere in the Twentieth Century: analyses of CO_2, climate and land use effects with four process-based ecosystem models *Glob. Biogeochem. Cycles* **15** 183–206

Michaletz S T, Cheng D, Kerkhoff A J and Enquist B J 2014 Convergence of terrestrial plant production across global climate gradients *Nature* doi:10.1038/nature13470

Purves D and Pacala S 2008 Predictive models of forest dynamics *Science* **320** 1452–3

Riahi K, Grübler A and Nakicenovic N 2007 Scenarios of long-term socio-economic and environmental development under climate stabilization *Technol. Forecast. Soc. Change* **74** 887–935

Schaphoff S, Lucht W, Gerten D, Sitch S, Cramer W and Prentice I 2006 Terrestrial biosphere carbon storage under alternative climate projections *Clim. Change* **74** 97–122

Scholze M, Knorr W, Arnell N W and Prentice I C 2006 A climate-change risk analysis for world ecosystems *Proc. Natl Acad. Sci.* **103** 13116–20

Sitch S *et al* 2003 Evaluation of ecosystem dynamics, plant geography and terrestrial carbon cycling in the LPJ dynamic global vegetation model *Glob. Change Biol.* **9** 161–85

Smith B, Prentice I C and Sykes M T 2001 Representation of vegetation dynamics in the modelling of terrestrial ecosystems: comparing two contrasting approaches within European climate space *Glob. Ecol. Biogeogr.* **10** 621–37

Smith B, Wårlind D, Arneth A, Hickler T, Leadley P, Siltberg J and Zaehle S 2014 Implications of incorporating N cycling and N limitations on primary production in an individual-based dynamic vegetation model *Biogeosciences* **11** 2027–54

Taylor K E, Stouffer R J and Meehl G A 2011 An Overview of CMIP5 and the experiment design *Bull. Am. Meteorol. Soc.* **93** 485–98

Thonicke K, Venevsky S, Sitch S and Cramer W 2001 The role of fire disturbance for global vegetation dynamics: coupling fire into a dynamic global vegetation model *Glob. Ecol. Biogeogr.* **10** 661–77

Wolf A, Ciais P, Bellassen V, Delbart N, Field C B and Berry J A 2011 Forest biomass allometry in global land surface models *Glob. Biogeochem. Cycles* **25** GB3015

Xia J, Luo Y, Wang Y-P and Hararuk O 2013 Traceable components of terrestrial carbon storage capacity in biogeochemical models *Glob. Change Biol.* **19** 2104–16